

1 ***Trypanosoma brucei* bloodstream forms depend upon uptake of *myo*-inositol for**
2 **Golgi phosphatidylinositol synthesis and normal cell growth**

3

4

5 Amaia González-Salgado^a, Michael Steinmann^a, Louise L. Major^b, Erwin Sigel^a,
6 Jean-Louis Reymond^c, Terry K. Smith^{b#} and Peter Bütikofer^{a#}

7

8 Institute of Biochemistry and Molecular Medicine, University of Bern, Bühlstrasse
9 28, 3012 Bern, Switzerland^a; Biomedical Sciences Research Complex, University of
10 St Andrews, North Haugh, St Andrews, Fife, KY16 9ST, UK^b; Department of
11 Chemistry and Biochemistry, University of Bern, Freiestrasse 3, 3012 Bern,
12 Switzerland^c

13

14 Running Title: *myo*-Inositol transport in bloodstream *T. brucei*

15

16 # Address correspondence to

17 Peter Bütikofer, Institute of Biochemistry and Molecular Medicine, University of
18 Bern, Bühlstrasse 28, 3012 Bern, Switzerland; peter.buetikofer@ibmm.unibe.ch

19 and

20 Terry K. Smith, Biomedical Sciences Research Complex, University of St Andrews,
21 North Haugh, St Andrews, Fife, KY16 9ST, UK; tks1@st-andrews.ac.uk

22

23

24 **ABSTRACT**

25 *myo*-Inositol is a building block for all inositol-containing phospholipids in
26 eukaryotes. It can be synthesized *de novo* from glucose-6-phosphate in the cytosol
27 and endoplasmic reticulum. Alternatively, it can be taken up from the environment
28 via Na⁺- or H⁺-linked *myo*-inositol transporters. While Na⁺-coupled *myo*-inositol
29 transporters are found exclusively in the plasma membrane, H⁺-linked *myo*-inositol
30 transporters are detected in intracellular organelles. In *Trypanosoma brucei*, the
31 causative agent of human African sleeping sickness, *myo*-inositol metabolism is
32 compartmentalized. *De novo* synthesized *myo*-inositol is used for
33 glycosylphosphatidylinositol production in the endoplasmic reticulum, whereas the
34 *myo*-inositol taken up from the environment is used for bulk phosphatidylinositol
35 synthesis in the Golgi. We now provide evidence that the Golgi localized *T. brucei*
36 H⁺-linked *myo*-inositol transporter (TbHMIT) is essential in bloodstream forms.
37 Down-regulation of TbHMIT expression by RNA interference blocked
38 phosphatidylinositol production and inhibited growth of parasites in culture.
39 Characterization of the transporter in a heterologous expression system demonstrated
40 a remarkable selectivity of TbHMIT for *myo*-inositol. It only tolerates a single
41 modification on the inositol ring, such as the removal of a hydroxyl group, or the
42 inversion of stereochemistry at a single hydroxyl group relative to *myo*-inositol.
43

44 INTRODUCTION

45 *myo*-Inositol is the precursor for all inositol-containing phospholipids, including
46 phosphatidylinositol (PI), phosphatidylinositol (poly)phosphates, inositol
47 phosphorylceramide (IPC) and glycosylphosphatidylinositol (GPI) in all eukaryotes.
48 In mammalian cells, it is taken up from the environment via sodium/*myo*-inositol
49 cotransporters (SMITs) or proton-linked *myo*-inositol transport (HMIT). Human
50 SMIT1 and SMIT2 belong to the sodium/glucose transporter family, SGLT/SLC5,
51 whose members in general mediate uptake of sugars and osmolytes in the
52 gastrointestinal tract and the kidney (1). They are localized in the plasma membrane
53 and, besides *myo*-inositol, also transport xylose and glucose (2, 3). In contrast, the
54 human HMIT belongs to the sugar/polyol transport facilitators family, GLUT/SLC2A
55 (4). While most members of this family are also located in the plasma membrane and
56 regulate sugar homeostasis within the body, subclass III transporters, to which HMIT
57 belongs, are typically localized intracellularly (5, 6). Interestingly,
58 GLUT12/SLC2A12 and HMIT/SLC2A13 have been found to co-localize with Golgi
59 markers (7, 8). Although the substrate specificities of the subclass III GLUT/SLC2A
60 transporters have been studied in model systems, their physiological roles have not
61 been firmly established (5, 6). Notably, HMIT completely lacks sugar transport
62 activity, but instead transports *myo*-inositol with a K_m of approximately 100 μ M in a
63 *Xenopus* oocyte expression system (8).

64 Alternatively to uptake, *myo*-inositol can be synthesized *de novo* in a reaction
65 sequence that is conserved from bacteria to mammals, using glucose-6-phosphate as
66 an initial substrate (9). Endogenously produced as well as imported *myo*-inositol can
67 then be used for inositol phospholipid synthesis in a process that is generally believed
68 to occur in the endoplasmic reticulum (ER). In yeast, plants, protozoa and mammals,

69 PI synthase has been localized to the ER using cell fractionation and
70 immunolocalization studies (10-13). Reconstitution experiments involving purified PI
71 synthase from *Saccharomyces cerevisiae* showed that it incorporates asymmetrically
72 into model vesicles, suggesting that its active site may face the cytosolic side of the
73 ER in yeast (10). However, the *in vivo* topology of the active site of PI synthase has
74 not been determined experimentally.

75 Interestingly, recent reports in protozoan parasites indicated that the Golgi
76 represents an additional site for inositol phospholipid synthesis. Direct evidence for
77 the presence of PI synthase in the Golgi was obtained from immunolocalization
78 studies in *T. brucei* bloodstream forms (13), showing that the enzyme has a dual
79 localization in the ER and Golgi. In support of the Golgi being the site of bulk PI
80 synthesis in trypanosomes (13), a subsequent study revealed that *T. brucei* procyclic
81 forms express a plasma membrane- and Golgi-localized proton-linked *myo*-inositol
82 transporter, TbHMIT (14). Down-regulation of TbHMIT inhibited bulk PI formation,
83 but had no effect on GPI synthesis, demonstrating that PI synthesis in *T. brucei* is
84 compartmentalized, with the Golgi representing the site of synthesis of bulk
85 membrane PI utilizing exogenous *myo*-inositol (14), and the ER being the site of PI
86 synthesis for GPI production utilizing *de novo* synthesized *myo*-inositol (15).
87 Transporter-mediated *myo*-inositol uptake has also been characterized in other
88 protozoan parasites, including *Leishmania donovani* (16-19) and *Trypanosoma cruzi*
89 (20, 21). These parasites all cause devastating human diseases, including
90 Leishmaniasis, Chagas disease and human African sleeping sickness. Membrane
91 transporters are of particular importance for these pathogens to acquire essential
92 nutrients from their respective hosts and offer attractive targets for rational drug
93 design and/or the delivery of cytotoxic substrate analogues. The reported dependence

94 of *T. brucei* procyclic forms in culture on exogenous *myo*-inositol (13, 14) validates
95 HMIT as potential drug target.

96 In this report, we extend our previous analysis of *myo*-inositol uptake in *T. brucei*
97 procyclic forms to the pharmacologically more relevant bloodstream form. We
98 demonstrate that the expression of TbHMIT is essential for normal growth of *T.*
99 *brucei* bloodstream parasites in culture and that it is involved in *myo*-inositol transport
100 and PI formation within the Golgi. In addition, we have tested a series of *myo*-inositol
101 stereoisomers and structural analogs and related compounds to characterize the
102 substrate specificity of TbHMIT.

103

104 MATERIALS AND METHODS

105 Unless otherwise stated, all reagents were of analytical grade and purchased from
106 Merck (Darmstadt, Germany), Sigma-Aldrich (Buchs, Switzerland) or ICN
107 Biomedicals (Tägerig, Switzerland). Antibiotics and fetal bovine serum (FBS) were
108 obtained from Invitrogen (Basel, Switzerland). Primers and sequencing services were
109 from Microsynth AG (Balgach, Switzerland). Restriction enzymes were purchased
110 from Thermo Scientific (Wohlen, Switzerland). *myo*-[2-³H(N)]inositol (15-20
111 Ci/mmol) (*myo*-[³H]inositol) and [³H]ethanolamine (40-60 Ci/mmol) were from
112 American Radiolabeled Chemicals (St. Louis, USA), and dCTP-[α -³²P] (3000
113 Ci/mmol) from PerkinElmer Life Sciences (Schwerzenbach, Switzerland).

114 *Trypanosomes and culture conditions* – Bloodstream form *T. brucei* derived from
115 MiTat 1.2, co-expressing T7 RNA polymerase and a tetracycline repressor (22), were
116 cultured at 37 °C with 5% CO₂ in HMI-9 (23) containing 10% heat-inactivated FBS
117 and 1 µg/ml G418. *T. brucei* strain 427 procyclic forms were cultured at 27 °C in
118 SDM-79 (24) containing 5% heat-inactivated FBS.

119 *RNAi-mediated gene silencing* – Expression of TbHMIT (Tb927.11.5350) was
120 down-regulated in *T. brucei* bloodstream forms by RNAi-mediated gene silencing
121 using a stem loop construct containing a phleomycin resistance gene. The stem-loop
122 was excised from plasmid pAG3020 (14) using BamHI and HindIII and re-ligated
123 into plasmid pMS1720RNAiBSF (25), resulting in plasmid pAG3020-BSF. Plasmid
124 extraction was performed using the Qiagen Plasmid Midi Kit (Qiagen, Hilden,
125 Germany) according to the manufacturer's instructions. Before transfection of *T.*
126 *brucei* bloodstream forms, plasmid DNA was linearized with NotI and precipitated
127 with phenol and chloroform.

128 *Generation of hemagglutinin (HA)-tagged TbHMIT* – Over-expression of C-
129 terminally 3xHA-tagged TbHMIT was performed using the inducible vector pALC14
130 as described previously (14), resulting in plasmid pAG3020-BSF2. Before
131 transfection of *T. brucei* bloodstream forms, plasmid DNA was linearized with NotI
132 and isolated with phenol and chloroform.

133 *Stable transfection of trypanosomes and selection of clones* – *T. brucei*
134 bloodstream forms ($4-5 \times 10^7$ cells) were harvested at mid-log phase ($0.8-1.1 \times 10^6$
135 cells/ml) by centrifugation at $1250 \times g$ for 10 min, suspended in 100 μ l of buffer (26)
136 (90 mM NaPO₄, 5 mM KCl, 0.15 mM CaCl₂, 50 mM HEPES pH 7.3) and mixed with
137 10 μ g of linearized plasmid pAG3020-BSF or pAG3020-BSF2. Electroporation was
138 performed in a 0.2 cm pulse cuvette (Bio-Rad Laboratories, Reinach, Switzerland)
139 with a Lonza Nucleofector System (Ruwag Lifescience, Bettlach, Switzerland) using
140 program FI-115. Electroporated cells were immediately inoculated in 10 ml of HMI-
141 9, containing 10% heat-inactivated FBS, and, if required for selection, 1 μ g/ml
142 phleomycin (for RNAi) or 0.1 μ g/ml puromycin (for over-expression). Clones were
143 obtained by limiting dilutions in 24-well plates in HMI-9, containing 10% heat-
144 inactivated FBS, in the presence of 1 μ g/ml phleomycin or 0.1 μ g/ml puromycin.
145 Antibiotic-resistant clones were tested for the presence of the introduced gene by
146 PCR. Expression of HA-tagged TbHMIT or induction of RNAi was started by
147 addition of 1 μ g/ml tetracycline to parasite cultures.

148 *RNA isolation and Northern blot analysis* – Total RNA for Northern blotting was
149 isolated using the Total SV RNA Extraction Kit (Promega, Dübendorf, Switzerland),
150 following the manufacturer's instructions. RNA (10 μ g) was separated on
151 formaldehyde-agarose gels (1% agarose, 2% formaldehyde in 3-N-morpholino
152 propane sulfonic acid) and transferred to GeneScreen Plus nylon membranes

153 (PerkinElmer Life Sciences). ³²P-Labeled probes were made by random priming the
154 same PCR products used as inserts in the stem-loop vector using the Prime-a-Gene
155 Labeling System (Promega). Hybridization was performed overnight at 60 °C in
156 hybridization buffer containing 7% (w/v) SDS, 1% (w/v) bovine serum albumin, 0.9
157 mM EDTA, 0.5 M Na₂HPO₄, pH 7.2, and the membrane was analyzed by
158 autoradiography using BioMax MS film and a TransScreen-HE intensifying screen.
159 Ribosomal RNA was visualized on the same formaldehyde-agarose gel by ethidium
160 bromide staining to control for equal loading.

161 *myo-Inositol uptake assays* – *T. brucei* bloodstream forms (1 x 10⁸ cells) at mid-
162 log phase were harvested by centrifugation at 1250 x g for 10 min and suspended in
163 phosphate-buffered saline (PBS; 135 mM NaCl, 1.3 mM KCl, 3.2 mM Na₂HPO₄, 0.5
164 mM KH₂PO₄, pH 7.4) at 27 °C. Uptake of *myo*-[³H]inositol was measured by adding
165 50 nM of *myo*-[³H]inositol to cells at 37 °C. At various time points, uptake of label
166 was terminated by pelleting 1.5 × 10⁷ parasites by centrifugation (1500 x g, 5 min, 4
167 °C) and washing three times in ice-cold PBS. After resuspension of the pellet in 100
168 µl PBS, radioactivity was measured by scintillation counting using a Packard Tri-
169 Carb 2100TR liquid scintillation analyzer (PerkinElmer Life Sciences). Aliquots of
170 the parasite suspensions before centrifugation were used to determine the total amount
171 of radioactivity in the assay.

172 *Metabolic labeling of trypanosomes, lipid extraction and thin layer*
173 *chromatography (TLC)* – Metabolic labeling of trypanosomes was performed as
174 described before (27). Briefly, *myo*-[³H]inositol was added to bloodstream or
175 procyclic form trypanosomes at mid-log phase, and incubation was continued for 16
176 h. Cells were harvested by centrifugation at 1750 x g for 10 min, washed with ice-
177 cold Tris-buffered saline (10 mM Tris, 144 mM NaCl, pH 7.4) to remove

178 unincorporated label, and bulk phospholipids were extracted twice with 10 ml
179 chloroform:methanol (CM; 2:1, by vol.). CM fractions were pooled, dried under
180 nitrogen and resuspended in a small volume of CM. Aliquots were treated with 6 µl
181 PI-specific phospholipase C from *Bacillus cereus* (Thermo Scientific, Wohlen,
182 Switzerland) for 60 min, as described elsewhere (28). Lipids were analyzed by TLC
183 on Silica Gel 60 plates (Merck) using solvent system 1 composed of
184 chloroform:methanol:acetic acid:water (25:15:4:2, by vol.) (29). Appropriate lipid
185 standards were run alongside the samples to be analyzed. Radioactivity was detected
186 by scanning the air-dried plate with a radioisotope detector (Berthold Technologies,
187 Regensdorf, Switzerland) and quantified using the Rita Star software provided by the
188 manufacturer. For analysis of GPI precursors, bloodstream form trypanosomes were
189 labeled for 16 h with trace amounts of [³H]ethanolamine (28). After harvesting the
190 cells and extracting bulk lipids as described above, GPI lipids were extracted from the
191 pellet using chloroform:methanol:water (10:10:3, by vol.) and partitioned between
192 water and butan-1-ol. [³H]-labeled GPI lipids in the butan-1-ol rich upper phase were
193 analyzed by TLC using solvent system 2 composed of chloroform:methanol:water
194 (10:10:3, by vol.) (28). Radioactivity was detected as above.

195 *Mass spectrometry and inositol analysis* - Total lipids for mass spectrometry
196 analysis were extracted using a modified Bligh and Dyer method (30). Briefly, *T.*
197 *brucei* bloodstream forms were collected at mid-log phase, washed with PBS,
198 resuspended in 100 µl of fresh PBS and transferred to a glass tube. 375 µl
199 chloroform:methanol (1:2, v/v) was then added and vortexed vigorously for 10-15
200 min. The sample was made biphasic by the addition of 125 µl chloroform and 125 µl
201 water, vortexed again and centrifuged at 1000 x g at RT for 5 min. The lower phase
202 was dried under nitrogen, and stored at 4 °C. Total lipid extracts were dissolved in 15

203 ml of chloroform:methanol (1:2, v/v) and 15 ml of acetonitrile:*iso*-propanol:water
204 (6:7:2, by vol.) and analysed with a Absceix 4000 QTrap, a triple quadrupole mass
205 spectrometer equipped with a nanoelectrospray source. Samples were delivered using
206 a Nanomate interface in direct infusion mode (~125 nl/min). Lipid extracts were
207 analyzed in both positive and negative ion modes using a capillary voltage of 1.25
208 kV. Tandem mass spectrometry (MS/MS) scanning (daughter, precursor and neutral
209 loss scans) was performed using nitrogen as the collision gas with collision energies
210 between 35-90 V. Each spectrum encompasses at least 50 repetitive scans. MS/MS
211 spectra were obtained with collision energies as follows: 35-45V, PC/SM in positive
212 ion mode, parent-ion scanning of m/z 184; 35-55V, PI in negative ion mode, parent-
213 ion scanning of m/z 241; 35-65V, PE in negative ion mode, parent-ion scanning of
214 m/z 196; 20-35V, PS in negative ion mode, neutral loss scanning of m/z 87; and 40-
215 90V. MS/MS daughter ion scanning was performed with collision energies between
216 35-90V. Assignment of phospholipid species is based upon a combination of survey,
217 daughter, precursor and neutral loss scans, as well previous assignments (31). The
218 identity of phospholipid peaks was verified using the LIPID MAPS: Nature
219 Lipidomics Gateway (www.lipidmaps.org).

220 For the inositol analysis, bloodstream forms were collected and lipids were
221 extracted as above. An internal standard of D₆ *myo*-inositol was added to samples
222 prior to hydrolysis by strong acid (6M HCl, 110 °C), derivatisation with TMS and
223 analysis by gas chromatography-mass spectrometry, as published elsewhere (32).
224 *myo*-Inositol was quantified and the mean and standard deviations of three separate
225 analyses were determined.

226 *Microscopy* – For immunolocalization of HA-tagged TbHMIT, trypanosomes
227 were cultured in the presence of tetracycline for 24 h to induce protein expression and

228 processed as described (14). HA-tagged proteins were detected using monoclonal
229 mouse anti-HA antibody (Covance, Munich, Germany) at a dilution of 1:250 in PBS
230 for 1 h at room temperature. Golgi was visualized by incubating fixed parasites for 1
231 h at room temperature with rabbit anti-TbGRASP antibody (kindly provided by G.
232 Warren, University of Vienna; used at a dilution of 1:1000). Subsequently, the slides
233 were washed three times with PBS and incubated with the corresponding secondary
234 antibodies, Alexa Fluor 594 goat anti-mouse IgG and Alexa Fluor 488 goat anti-rabbit
235 IgG (Invitrogen) at a dilution of 1:1000 and 1:500, respectively, for 1 h at room
236 temperature. Slides were washed three times with PBS and mounted using
237 Vectashield containing 4',6'-diamidino-2-phenylindol (DAPI; Vector Laboratories,
238 Burlingame, USA). Fluorescence microscopy was performed on a Leica AF6000
239 microscope (Leica Microsystems, Heerbrugg, Switzerland), using the software
240 provided by the manufacturer.

241 *Substrate specificity of TbHMIT* – *Xenopus laevis* oocytes were prepared,
242 injected with Tb927.11.5350 cRNA and defolliculated as described previously (14).
243 Electrophysiological experiments were performed as described before (14). *myo*-
244 Inositol, *epi*-quercitol, *vibo*-quercitol, *proto*-quercitol, *scyllo*-inositol, *muco*-inositol,
245 *allo*-inositol, *epi*-inositol, 1D-*chiro*-inositol, 1L-*chiro*-inositol, 1L-*epi*-2-inosose,
246 phytic acid, L-quebrachitol, D-pinitol, N-00601 ((1R,4S)-6-methoxycyclohexane-
247 1,2,3,4,5-pentol), N-50350 ((1R,3S)-6-methoxycyclohexane-1,2,3,4,5-pentol) and D-
248 *myo*-inositol-3-phosphate at 200 μ M were applied for 20 s for each measurement.
249 Potential inhibition of TbHMIT was tested by applying a combination of 200 μ M
250 *myo*-inositol and one of the compounds described above at an equal concentration.
251 The resulting signal was compared with that elicited by 200 μ M *myo*-inositol alone.

252

253 RESULTS AND DISCUSSION

254 *Characterization of T. brucei TbHMIT in bloodstream form parasites* – To study
255 if TbHMIT is essential in *T. brucei* bloodstream forms in culture, we generated
256 tetracycline-inducible RNAi cell lines against Tb927.11.5350. Transfection of *T.*
257 *brucei* bloodstream forms with plasmid pAG3020-BSF and selection by resistance to
258 phleomycin resulted in several clones, one of which (A3) was selected for all
259 subsequent experiments. After 2 days of induction of RNAi by addition of
260 tetracycline to the culture, parasite growth decreased compared to uninduced (control)
261 cells (Fig. 1A). Northern blot analysis showed that after 2 days of RNAi,
262 Tb927.11.5350 mRNA was undetectable (Fig. 1A, inset). The uptake of *myo*-inositol
263 into bloodstream form RNAi parasites was measured by adding trace amounts of
264 *myo*-[³H]inositol to trypanosomes cultured for 2 days in the absence or presence of
265 tetracycline and measuring radioactivity in the cell pellets after centrifugation. The
266 results show that uptake of *myo*-[³H]inositol into control trypanosomes increased
267 linearly over 90 min (Fig. 1B). A similar time-dependent linear increase in cell-
268 associated radioactivity was also observed for RNAi parasites after down-regulation
269 of TbHMIT, however, uptake of *myo*-[³H]inositol was reduced to approximately half
270 of that in control cells. To demonstrate that the *myo*-[³H]inositol that was taken up
271 was being metabolized into inositol-containing phospholipids, bloodstream forms
272 cultured in the absence or presence of tetracycline were incubated for 16 h in the
273 presence of *myo*-[³H]inositol followed by analysis of radiolabeled lipids by TLC and
274 radioactivity scanning. In the absence of tetracycline, a single [³H]-labeled lipid class
275 was detected (Fig. 1C top panel, and Fig. S1A), which was identified as [³H]PI based
276 on its co-migration with a commercial PI standard and complete susceptibility to PI-
277 specific phospholipase C (Fig. S1B). In parasites after RNAi-mediated down-

278 regulation of TbHMIT, formation of [³H]PI was reduced by >85% (Fig. 1C, middle
279 panel). No formation of [³H]inositol phosphorylceramide ([³H]IPC), which is readily
280 labeled in procyclic forms (Fig. 1C; bottom panel; see also (14)), was observed in un-
281 induced bloodstream forms. This observation is consistent with previous reports
282 showing that IPC synthesis in *T. brucei* bloodstream forms is largely absent (31, 33).
283 In addition, we analyzed the formation of GPI precursor lipids by labeling
284 bloodstream form parasites cultured in the absence or presence of tetracycline with
285 [³H]ethanolamine, which gets incorporated into GPIs (28). As shown in Fig. 1D,
286 formation of the major ³H-labeled GPI precursors, P2 and P3, was readily observed in
287 parasites after depletion of TbHMIT. This result demonstrates that, as previously
288 shown in procyclic forms (14), GPI synthesis is not affected by down-regulation of
289 TbHMIT.

290 The effect of TbHMIT RNAi on parasite lipid composition was investigated by
291 extracting the lipids and analyzing them by ES-MS. In negative ion mode a range of
292 peaks was observed in the un-induced RNAi cells, corresponding to the phospholipid
293 profile of wild-type parasites (Fig. 2A; see (31) for comparison). These include the
294 major plasmalogen (alk-enyl acyl) phosphatidylethanolamine (PE) species at 727 m/z,
295 and PI molecular species at 865, 887 and 913 m/z, corresponding to 36:0, 38:3, and
296 40:4 PI. Upon induction of the RNAi cells for 48 hours with tetracycline (Fig. 2B),
297 the intensity of all PI molecular species clearly diminished compared to un-induced
298 cells, while the plasmalogen PE is still the dominant species (compare Fig. 2A with
299 Fig. 2B). To confirm the decrease in the PI molecular species, parent ion scans of 241
300 m/z (collision-induced inositol-1,2-cyclic phosphate fragment) were recorded (Fig.
301 S2). In extracts of un-induced cells all major PI species are clearly detected (Fig.
302 S2A). In contrast, in extracts from parasites after 48 h of tetracycline induction the

303 intensities of these fragments are drastically decreased (Fig. S2B). In addition, the
304 amounts of inositol-containing phospholipids were quantified by measuring the *myo*-
305 inositol contents in lipid extracts from control and induced cells and normalizing to
306 cell numbers. The results show that RNAi cells after down-regulation of TbHMIT
307 only had $79.5 \pm 2.5\%$ of *myo*-inositol-containing lipids compared to non-induced cells
308 ($100 \pm 4\%$; mean values \pm standard deviations from three independent experiments).

309 In the induced cells, apart from the reduction in PI species, the intensities of two
310 phospholipid species at 762 and 795 m/z had increased (Fig. 2B). These two species
311 were subjected to fragmentation (Fig. S3A and Fig. S3B, respectively) and identified
312 as PS 34:0 and PG 38:5, respectively. The only other obvious change in the
313 phospholipids was observed in positive ion mode (Fig. S4), which shows the choline-
314 phosphate containing species of phosphatidylcholine (PC) and sphingomyelin (SM).
315 The species at 794 m/z, representing PC 40:4, is clearly decreased in cells after
316 TbHMIT RNAi compared to un-induced cells (compare Fig. S4A with Fig. S4B). The
317 cells are obviously trying to compensate for a lack of PI, but the reasons for these
318 specific changes are unknown, other than to maintain the correct membrane fluidity
319 for normal cellular functions.

320 *Localization of TbHMIT in T. brucei bloodstream forms – Immunofluorescence*
321 microscopy revealed that ectopically expressed HA-tagged TbHMIT in *T. brucei*
322 bloodstream forms localized to a distinct intracellular structure located between the
323 nucleus and the kinetoplast (Fig. 3). The signal completely co-localized with
324 TbGRASP (Fig. 3), a marker for the Golgi in *T. brucei* (34). These findings are in line
325 with a previous report showing that TbHMIT localizes to the Golgi in *T. brucei*
326 procyclic forms (14).

327 The Golgi localization of TbHMIT in *T. brucei* bloodstream forms is noteworthy.
328 It is believed that PI synthesis occurs on the cytosolic side of the ER (10, 35). It
329 should be noted, however, that in several studies in plants (11), yeast (36), protozoa
330 (13) and mammalian cells (12), PI synthase was found to localize not only in the ER,
331 but also in close proximity to or in the Golgi. As has been demonstrated in *T. brucei*
332 (13, 14), PI synthesis in the ER and Golgi may serve different purposes. PI production
333 in the ER is required for GPI synthesis, while PI produced in the Golgi provides bulk
334 PI for membrane formation. Based on the localization of TbHMIT in the Golgi, these
335 results suggest that the last step in PI synthesis, i.e. the attachment of *myo*-inositol to
336 CDP-diacylglycerol (CDP-DAG), may occur in the lumen of the Golgi. Interestingly,
337 a recent report showed that *T. brucei* CDP-DAG synthase localizes to the ER/Golgi
338 (37), which would be consistent with PI synthesis taking place in the lumen of the ER
339 and Golgi. In addition, membrane topology prediction programs indicate that the
340 active site of *T. brucei* PI synthase is on the luminal side of the ER. Based on these
341 observations we propose the following model for compartmentalization of PI
342 synthesis in *T. brucei* (Fig. 4). In procyclic forms, *myo*-inositol is taken up from the
343 environment via plasma membrane localized TbHMIT; in bloodstream forms, *myo*-
344 inositol uptake likely occurs via a different transporter. Cytosolic *myo*-inositol is then
345 transported into the Golgi via TbHMIT, where it is used for bulk PI and,
346 subsequently, IPC synthesis. In contrast, *de novo* synthesis of *myo*-inositol starts with
347 the cytosolic conversion of glucose-6-phosphate to inositol-3-phosphate, which in
348 turn is transported into the ER via an unknown transporter. After dephosphorylation,
349 newly synthesized *myo*-inositol is used for PI formation by PI synthase. Subsequently,
350 PI is translocated from the luminal to the cytosolic face of the ER, where it is used to
351 initiate GPI synthesis. Recently, a similar mechanism has also been proposed to occur

352 in the intra-erythrocytic stage of the malaria parasite, *Plasmodium falciparum* (38). In
353 addition, it is worth mentioning that the two PI synthase isoforms described in
354 *Arabidopsis thaliana* show different substrate specificities (11), suggesting that two
355 pools of PI may exist and that these may enter alternative routes of metabolism.
356 Furthermore, a Golgi localization of PI synthase (11-12, 36) and HMIT (8) has also
357 been documented in other cells. Thus, we propose that PI formation and metabolism
358 may be similarly compartmentalized in other eukaryotes as well.

359 Our data using exogenously added *myo*-[³H]inositol showed that after depletion
360 of TbHMIT by RNAi, uptake of *myo*-[³H]inositol into bloodstream form parasites still
361 occurred, albeit at a clearly reduced level (Fig. 1B), yet the formation of [³H]PI was
362 blocked (Fig. 1C). Together with the observed localization of TbHMIT in the Golgi,
363 these data suggest that *myo*-[³H]inositol may be taken up in *T. brucei* bloodstream
364 forms via a different transporter, located in the plasma membrane, and subsequently
365 remains metabolically inactive because of the lack of the Golgi-localized TbHMIT,
366 preventing entry of (cytosolic) *myo*-[³H]inositol into the Golgi for [³H]PI production.
367 These results differ slightly from our previous findings in *T. brucei* procyclic forms
368 (14), where RNAi against TbHMIT not only blocked [³H]PI formation but also *myo*-
369 [³H]inositol uptake into parasites. Interestingly, in procyclic forms TbHMIT is not
370 only present in the Golgi but can also be detected in the plasma membrane, mediating
371 *myo*-[³H]inositol uptake into the cell. We are currently addressing these differences
372 between bloodstream and procyclic forms with further experiments.

373 Collectively, these results demonstrate that expression of TbHMIT is essential for
374 normal growth of *T. brucei* bloodstream forms in culture and that it is involved in
375 *myo*-inositol transport into the Golgi for PI formation within the lumen of the Golgi.

376 *Substrate Specificity of TbHMIT* – Perfusion of TbHMIT-expressing *Xenopus*
377 *laevis* oocytes with 200 μ M *myo*-inositol resulted in inward currents of 20 ± 1 nA
378 (mean value \pm standard deviations using 13 oocytes from two independent batches).
379 The same concentration of *myo*-inositol did not elicit any currents in water-injected
380 control oocytes. These results are consistent with a previous report (14). To identify
381 other potential substrates, oocytes expressing TbHMIT were exposed to a series of
382 commercially available compounds that are structurally related to *myo*-inositol (Fig.
383 5). The currents elicited by these compounds (each applied at a concentration of 200
384 μ M) were compared to those obtained with *myo*-inositol (Fig. 6). Interestingly, we
385 found that two quercitol isomers, *epi*- and *vibo*-quercitol, elicited currents comparable
386 to those induced by *myo*-inositol ($76 \pm 9\%$ and $83 \pm 3\%$, respectively, of the *myo*-
387 inositol current). In contrast, $<5\%$ of the current obtained with *myo*-inositol was
388 elicited by another quercitol isomer, *proto*-quercitol (Fig. 6). Quercitols comprise a
389 group of 6-C-containing polyols, which compared to the group of inositol isomers
390 lack one hydroxyl group (Fig. 5) and in the case of *proto*-quercitol, contain a C1
391 epimerisation. In addition, small currents (15-25% of the *myo*-inositol current) were
392 also obtained with *scyllo*-inositol, *epi*-inositol, 1L-*chiro*-inositol and phytic acid
393 (*myo*-inositol-1,2,3,4,5,6-hexakisphosphate). In contrast, the currents induced by
394 *muco*-inositol, *allo*-inositol, 1D-*chiro*-inositol, 1L-*epi*-2-inosose (2L-2,3,4,6/5-
395 pentahydroxycyclohexanone), L-quebrachitol (2-O-methyl-L-*chiro*-inositol), D-
396 pinitol (3-O-methyl-D-*chiro*-inositol), N-00601 ((1R,4S)-6-methoxycyclohexane-
397 1,2,3,4,5-pentol), N-50350 ((1R,3S)-6-methoxycyclohexane-1,2,3,4,5-pentol) and D-
398 inositol-3-phosphate were $<5\%$ of the control *myo*-inositol current (Fig. 6).

399 Together, these results provide an insight into the selectivity of the transporter in
400 terms of functional groups and stereoselectivity. Among the different analogs tested,

401 deleting a single hydroxyl group at the 1 (as in (-)-*vibo*-quercitol) or 6 position (as in
402 (+)-*epi*-quercitol) only induced a small decrease in current activity. Inversion of
403 stereochemistry at a single hydroxyl group relative to *myo*-inositol was also partly
404 tolerated, leaving 10-25% of current activity as in *scyllo*-inositol, *epi*-inositol, 1L-
405 *chiro*-inositol and 1D-*chiro*-inositol. However a double modification of inositol in
406 terms of inversion of stereochemistry and substitution (deoxy- or methyl ether)
407 essentially suppressed all current activity, as in quebrachitol, (+)-*proto*-quercitol,
408 *muco*-inositol, *allo*-inositol and D-pinitol. Note that 1L-*epi*-2-inosose, which features
409 a carbonyl group at position 4 of inositol, showed no transporter activity, and that
410 simple carbohydrates such as glucose, galactose and mannose, which are also
411 structurally related to inositol, were not accepted by the transporter (see (14)). In
412 addition, all compounds were analysed for their potential to inhibit TbHMIT-
413 mediated *myo*-inositol transport in *Xenopus* oocytes. Co-application with *myo*-inositol
414 showed that none of compounds affected the *myo*-inositol-elicited currents,
415 demonstrating that at the concentrations tested they did not act as inhibitors of
416 TbHMIT. Finally, to establish the apparent affinities of TbHMIT for transport of *epi*-
417 and *vibo*-quercitol, *Xenopus* oocytes were exposed to increasing concentrations of the
418 compounds and currents were recorded. The results showed that the EC₅₀ values for
419 *epi*- and *vibo*-quercitol (121 μM and 104 μM, respectively; mean values from 2
420 independent experiments) were in the same range as that for *myo*-inositol (61 μM; see
421 (14)).

422 Together, these data show that TbHMIT is remarkably selective for *myo*-inositol.
423 It tolerates a single modification on the inositol ring only, such as the removal of a
424 hydroxyl group at the 1- or 6-position or the inversion of stereochemistry at a single
425 hydroxyl group relative to *myo*-inositol, but no additional modifications. Interestingly,

426 TbHMIT (14) and its orthologs from *T. cruzi* (20) and *Leishmania* parasites (18, 39)
427 show no transport activity for monosaccharides. This is in marked contrast to all other
428 members of the GLUT/SLC2A family, including the intracellularly located members
429 of the subclass III, which transport many different monosaccharides (1, 5, 6). In
430 addition, HMIT's transport specificity is also different from that of the SMITs, which
431 transport both *myo*-inositol and monosaccharides (2, 3).

432

433 **ACKNOWLEDGEMENTS**

434 This work was supported by Swiss National Science Foundation Sinergia grant
435 CRSII3_141913 to PB and ES, Wellcome Trust grant 093228 to TKS, and the NCCR
436 TransCure support to JLR. *D-myo*-inositol-3-phosphate was prepared by Lloyd Sayer
437 (University of St Andrews). PB thanks M. Bütikofer for support, A.K. Menon for
438 discussions and I. Dragons for stimulation.

439

440

441 **ABBREVIATIONS**

442 ER, endoplasmic reticulum; ES-MS, electrospray-mass spectrometry; GPI,
443 glycosylphosphatidylinositol; HA, hemagglutinin; HMIT, proton-linked *myo*-inositol
444 transporter; IPC, inositol phosphorylceramide; MS/MS, tandem mass spectrometry;
445 PC, phosphatidylcholine; PE, phosphatidylethanolamine; PI, phosphatidylinositol; PS,
446 phosphatidylserine; SM, sphingomyelin; SMIT, sodium/*myo*-inositol cotransporters;
447 TLC, thin layer chromatography

448

449 **REFERENCES**

- 450 1. **Wright EM, Loo DD, Hirayama BA.** 2011. Biology of human sodium
451 glucose transporters. *Physiol Rev* **91**:733-94.
- 452 2. **Hager K, Hazama A, Kwon HM, Loo DD, Handler JS, Wright EM.** 1995.
453 Kinetics and specificity of the renal Na⁺/*myo*-inositol cotransporter expressed
454 in *Xenopus* oocytes. *J Membr Biol* **143**:103-13.
- 455 3. **Coady MJ, Wallendorff B, Gagnon DG, Lapointe JY.** 2002. Identification
456 of a novel Na⁺/*myo*-inositol cotransporter. *J Biol Chem* **277**:35219-24.
- 457 4. **Joost HG, Bell GI, Best JD, Birnbaum MJ, Charron MJ, Chen YT, Doege
458 H, James DE, Lodish HF, Moley KH, Moley JF, Mueckler M, Rogers S,
459 Schurmann A, Seino S, Thorens B.** 2002. Nomenclature of the
460 GLUT/SLC2A family of sugar/polyol transport facilitators. *Am J Physiol*
461 *Endocrinol Metab* **282**:E974-6.
- 462 5. **Augustin R.** 2010. The protein family of glucose transport facilitators: It's not
463 only about glucose after all. *IUBMB Life* **62**:315-33.
- 464 6. **Cura AJ, Carruthers A.** 2012. Role of monosaccharide transport proteins in
465 carbohydrate assimilation, distribution, metabolism, and homeostasis. *Compr*
466 *Physiol* **2**:863-914.
- 467 7. **Flessner LB, Moley KH.** 2009. Similar [DE]XXXL[LI] motifs differentially
468 target GLUT8 and GLUT12 in Chinese hamster ovary cells. *Traffic* **10**:324-
469 33.
- 470 8. **Di Daniel E, Mok MH, Mead E, Mutinelli C, Zambello E, Caberlotto LL,
471 Pell TJ, Langmead CJ, Shah AJ, Duddy G, Kew JN, Maycox PR.** 2009.
472 Evaluation of expression and function of the H⁺/*myo*-inositol transporter
473 HMIT. *BMC Cell Biol* **10**:54.

- 474 9. **Michell RH.** 2013. Inositol lipids: from an archaeal origin to
475 phosphatidylinositol 3,5-bisphosphate faults in human disease. *Febs J*
476 **280**:6281-94.
- 477 10. **Fischl AS, Homann MJ, Poole MA, Carman GM.** 1986.
478 Phosphatidylinositol synthase from *Saccharomyces cerevisiae*. Reconstitution,
479 characterization, and regulation of activity. *J Biol Chem* **261**:3178-83.
- 480 11. **Löfke C, Ischebeck T, König S, Freitag S, Heilmann I.** 2008. Alternative
481 metabolic fates of phosphatidylinositol produced by phosphatidylinositol
482 synthase isoforms in *Arabidopsis thaliana*. *Biochem J* **413**:115-24.
- 483 12. **Batenburg JJ, Klazinga W, van Golde LM.** 1985. Regulation and location
484 of phosphatidylglycerol and phosphatidylinositol synthesis in type II cells
485 isolated from fetal rat lung. *Biochim Biophys Acta* **833**:17-24.
- 486 13. **Martin KL, Smith TK.** 2006. Phosphatidylinositol synthesis is essential in
487 bloodstream form *Trypanosoma brucei*. *Biochem J* **396**:287-95.
- 488 14. **Gonzalez-Salgado A, Steinmann ME, Greganova E, Rauch M, Mäser P,**
489 **Sigel E, Bütikofer P.** 2012. *myo*-Inositol uptake is essential for bulk inositol
490 phospholipid but not glycosylphosphatidylinositol synthesis in *Trypanosoma*
491 *brucei*. *J Biol Chem* **287**:13313-23.
- 492 15. **Martin KL, Smith TK.** 2006. The glycosylphosphatidylinositol (GPI)
493 biosynthetic pathway of bloodstream-form *Trypanosoma brucei* is dependent
494 on the *de novo* synthesis of inositol. *Mol Microbiol* **61**:89-105.
- 495 16. **Drew ME, Langford CK, Klamo EM, Russell DG, Kavanaugh MP,**
496 **Landfear SM.** 1995. Functional expression of a *myo*-inositol/H⁺ symporter
497 from *Leishmania donovani*. *Mol Cell Biol* **15**:5508-15.

- 498 17. **Klamo EM, Drew ME, Landfear SM, Kavanaugh MP.** 1996. Kinetics and
499 stoichiometry of a proton/*myo*-inositol cotransporter. *J Biol Chem* **271**:14937-
500 43.
- 501 18. **Seyfang A, Landfear SM.** 2000. Four conserved cytoplasmic sequence
502 motifs are important for transport function of the *Leishmania* inositol/H⁺
503 symporter. *J Biol Chem* **275**:5687-93.
- 504 19. **Mongan TP, Ganapasam S, Hobbs SB, Seyfang A.** 2004. Substrate
505 specificity of the *Leishmania donovani myo*-inositol transporter: critical role
506 of inositol C-2, C-3 and C-5 hydroxyl groups. *Mol Biochem Parasitol*
507 **135**:133-41.
- 508 20. **Einicker-Lamas M, Almeida AC, Todorov AG, de Castro SL, Caruso-**
509 **Neves C, Oliveira MM.** 2000. Characterization of the *myo*-inositol transport
510 system in *Trypanosoma cruzi*. *Eur J Biochem* **267**:2533-7.
- 511 21. **Einicker-Lamas M, Nascimento MT, Masuda CA, Oliveira MM, Caruso-**
512 **Neves C.** 2007. *Trypanosoma cruzi* epimastigotes: regulation of *myo*-inositol
513 transport by effectors of protein kinases A and C. *Exp Parasitol* **117**:171-7.
- 514 22. **Wirtz E, Leal S, Ochatt C, Cross GM.** 1999. A tightly regulated inducible
515 expression system for conditional gene knock-outs and dominant-negative
516 genetics in *Trypanosoma brucei*. *Mol Biochem Parasitol* **99**:89-101.
- 517 23. **Shlomai J.** 2004. The structure and replication of kinetoplast DNA. *Curr Mol*
518 *Med* **4**:623-47.
- 519 24. **Brun R, Schönenberger M.** 1979. Cultivation and *in vitro* cloning or
520 procyclic culture forms of *Trypanosoma brucei* in a semi-defined medium.
521 *Acta Trop* **36**:289-92.

- 522 25. **Serricchio M, Bütikofer P.** 2013. Phosphatidylglycerophosphate synthase
523 associates with a mitochondrial inner membrane complex and is essential for
524 growth of *Trypanosoma brucei*. *Mol Microbiol* **87**:569-79.
- 525 26. **Schumann Burkard G, Jutzi P, Roditi I.** 2011. Genome-wide RNAi screens
526 in bloodstream form trypanosomes identify drug transporters. *Mol Biochem*
527 *Parasitol* **175**:91-4.
- 528 27. **Bütikofer P, Ruepp S, Boschung M, Roditi I.** 1997. 'GPEET' procyclin is
529 the major surface protein of procyclic culture forms of *Trypanosoma brucei*
530 *brucei* strain 427. *Biochem J* **326**:415-423.
- 531 28. **Mayor S, Menon AK, Cross GA.** 1990. Glycolipid precursors for the
532 membrane anchor of *Trypanosoma brucei* variant surface glycoproteins. II.
533 Lipid structures of phosphatidylinositol-specific phospholipase C sensitive and
534 resistant glycolipids. *J Biol Chem* **265**:6174-81.
- 535 29. **Bütikofer P, Lin ZW, Kuypers FA, Scott MD, Xu CM, Wagner GM, Chiu**
536 **DT, Lubin B.** 1989. Chlorpromazine inhibits vesiculation, alters
537 phosphoinositide turnover and changes deformability of ATP-depleted RBCs.
538 *Blood* **73**:1699-704.
- 539 30. **Bligh EG, Dyer WJ.** 1959. A rapid method of total lipid extraction and
540 purification. *Can J Biochem Physiol* **37**:911-7.
- 541 31. **Richmond GS, Gibellini F, Young SA, Major L, Denton H, Lilley A,**
542 **Smith TK.** 2010. Lipidomic analysis of bloodstream and procyclic form
543 *Trypanosoma brucei*. *Parasitology* **137**:1357-92.
- 544 32. **Ferguson MAJ.** 1993. GPI membrane anchors: isolation and analysis, p. 349-
545 383. *In* Fukuda M and Kobata A (ed.), *Glycobiology: a practical approach*,
546 vol. 125. IRL Press at Oxford University Press.

- 547 33. **Sutterwala SS, Hsu FF, Sevova ES, Schwartz KJ, Zhang K, Key P, Turk**
548 **J, Beverley SM, Bangs JD.** 2008. Developmentally regulated sphingolipid
549 synthesis in African trypanosomes. *Mol Microbiol* **70**:281-96.
- 550 34. **He CY, Ho HH, Malsam J, Chalouni C, West CM, Ullu E, Toomre D,**
551 **Warren G.** 2004. Golgi duplication in *Trypanosoma brucei*. *J Cell Biol*
552 **165**:313-21.
- 553 35. **Nikawa J, Yamashita S.** 1997. Phosphatidylinositol synthase from yeast.
554 *Biochim Biophys Acta* **1348**:173-8.
- 555 36. **Leber A, Hrastnik C, Daum G.** 1995. Phospholipid-synthesizing enzymes in
556 Golgi membranes of the yeast, *Saccharomyces cerevisiae*. *FEBS Lett*
557 **377**:271-4.
- 558 37. **Lilley AC, Major L, Young S, Stark MJ, Smith TK.** 2014. The essential
559 roles of cytidine diphosphate-diacylglycerol synthase in bloodstream form
560 *Trypanosoma brucei*. *Mol Microbiol* **92**:453-70.
- 561 38. **Macrae JI, Lopaticki S, Maier AG, Rupasinghe T, Nahid A, Cowman AF,**
562 **McConville MJ.** 2014. *Plasmodium falciparum* is dependent on *de novo* myo-
563 inositol biosynthesis for assembly of GPI glycolipids and infectivity. *Mol*
564 *Microbiol* **91**:762-76.
- 565 39. **Seyfang A, Kavanaugh MP, Landfear SM.** 1997. Aspartate 19 and
566 glutamate 121 are critical for transport function of the *myo*-inositol/H⁺
567 symporter from *Leishmania donovani*. *J Biol Chem* **272**:24210-5.
- 568
- 569
- 570

571 **FIGURE LEGENDS**

572 **Figure 1. Essentiality of TbHMIT in *T. brucei* bloodstream forms.** (A) Growth of
573 *T. brucei* bloodstream form RNAi parasites. Expression of TbHMIT in *T. brucei*
574 bloodstream forms was down-regulated by tetracycline-inducible RNAi, and growth
575 of trypanosomes was monitored for 5 days. Data points represent cumulative cell
576 numbers of RNAi cells incubated in the absence (filled symbols) or presence (open
577 symbols) of tetracycline and correspond to mean values \pm standard deviations from
578 three experiments using clone A3. The *inset* shows a Northern blot analysis of total
579 RNA extracted from trypanosomes after 2 days of incubation in the absence (-) or
580 presence (+) of tetracycline (Tet) and probed with [³²P]-labeled oligonucleotides used
581 as inserts for the respective stem-loop vector (*top panel*); rRNA was stained with
582 ethidium bromide and used as loading control (*bottom panel*). Two other RNAi clones
583 showed similar growth defects and reductions in TbHMIT mRNA levels upon
584 treatment with tetracycline. (B) *myo*-inositol uptake by *T. brucei* bloodstream forms.
585 After 2 days of incubation in the absence (filled symbols) or presence (open symbols)
586 of tetracycline, RNAi parasites (clone A3) were washed and subsequently incubated
587 with trace amounts of *myo*-[³H]inositol (50 nM, final concentration). After indicated
588 times, parasites were washed, and the amount of radioactivity in the cell pellet was
589 measured. Uptake of *myo*-[³H]inositol at each time point was calculated and plotted as
590 a function of incubation time. Data points represent mean values \pm standard
591 deviations of triplicate determinations from three independent experiments. (C)
592 Analysis of *myo*-[³H]inositol-labeled lipids. *T. brucei* bloodstream form TbHMIT
593 RNAi cells (clone A3) were incubated in the absence or presence of tetracycline for 3
594 days. During the last 16 h of incubation, parasites (2×10^8 cells) were labeled with 25
595 μ Ci of *myo*-[³H]inositol. [³H]-labeled lipids were extracted from parasites incubated

596 in the absence (top panel) or presence (middle panel) of tetracycline to down-regulate
597 TbHMIT, separated by one-dimensional TLC using solvent system 1, and visualized
598 by scanning the plate (14). Extracts from equal cell equivalents were applied. The
599 bottom panel represents extracts from *T. brucei* procyclic forms run on the same TLC
600 plate for comparison, indicating the migration of [³H]inositol phosphorylceramide
601 ([³H]IPC) and [³H]phosphatidylinositol ([³H]PI). The vertical lines indicate the site of
602 sample application (left line) and the migration of the solvent front (right line),
603 respectively. (D) Analysis of [³H]ethanolamine-labeled GPI lipids. Trypanosomes
604 were cultured in the absence (top panel) or presence (middle panel) of tetracycline for
605 2 days to down-regulate TbHMIT, and then labeled during 16 h with
606 [³H]ethanolamine. [³H]GPI lipids were extracted and analyzed by TLC using solvent
607 system 2. The major GPI lipids, designated P2 and P3, were identified based on
608 published R_f values (28) and the migration of [³H]-labeled PP1, i.e. the major GPI
609 precursor lipid in *T. brucei* procyclic forms, run on the same plate (bottom panel). The
610 migration of residual [³H]PE is also indicated. The vertical lines indicate the site of
611 sample application (left line) and the migration of the solvent front (right line),
612 respectively.

613 **Figure 2. Phospholipid analysis of *T. brucei* bloodstream form TbHMIT RNAi**
614 **cells.** Lipid extracts from parasites incubated in the absence (A) or presence (B) of
615 tetracycline for 48 hours were analyzed by negative ion ES-MS survey scans (600-
616 1000 m/z (mass/charge)). The major phospholipid classes are annotated: PI,
617 phosphatidylinositol; PE, phosphatidylethanolamine; EPC, ethanolamine
618 phosphorylceramide. The arrows in (B) refer to the phospholipid species that increase
619 or decrease after RNAi against TbHMIT compared to non-induced cells (A).

620 **Figure 3. Localization of TbHMIT in *T. brucei* bloodstream forms.** Trypanosomes
621 cultured in the presence of tetracycline for 24 h to induce expression of HA-tagged
622 TbHMIT were washed, allowed to settle onto microscope slides, fixed with
623 paraformaldehyde, and permeabilized with Triton X-100. TbHMIT was detected
624 using anti-HA antibody (first panel) whereas the Golgi was stained with anti-GRASP
625 antibody (second panel). The third panel shows an overlay of panels A and B, with
626 DNA stained with DAPI. The corresponding differential interference contrast (DIC)
627 micrograph is shown in the fourth panel.

628 **Figure 4. Schematic of compartmentalized *myo*-inositol metabolism in *T. brucei*.**

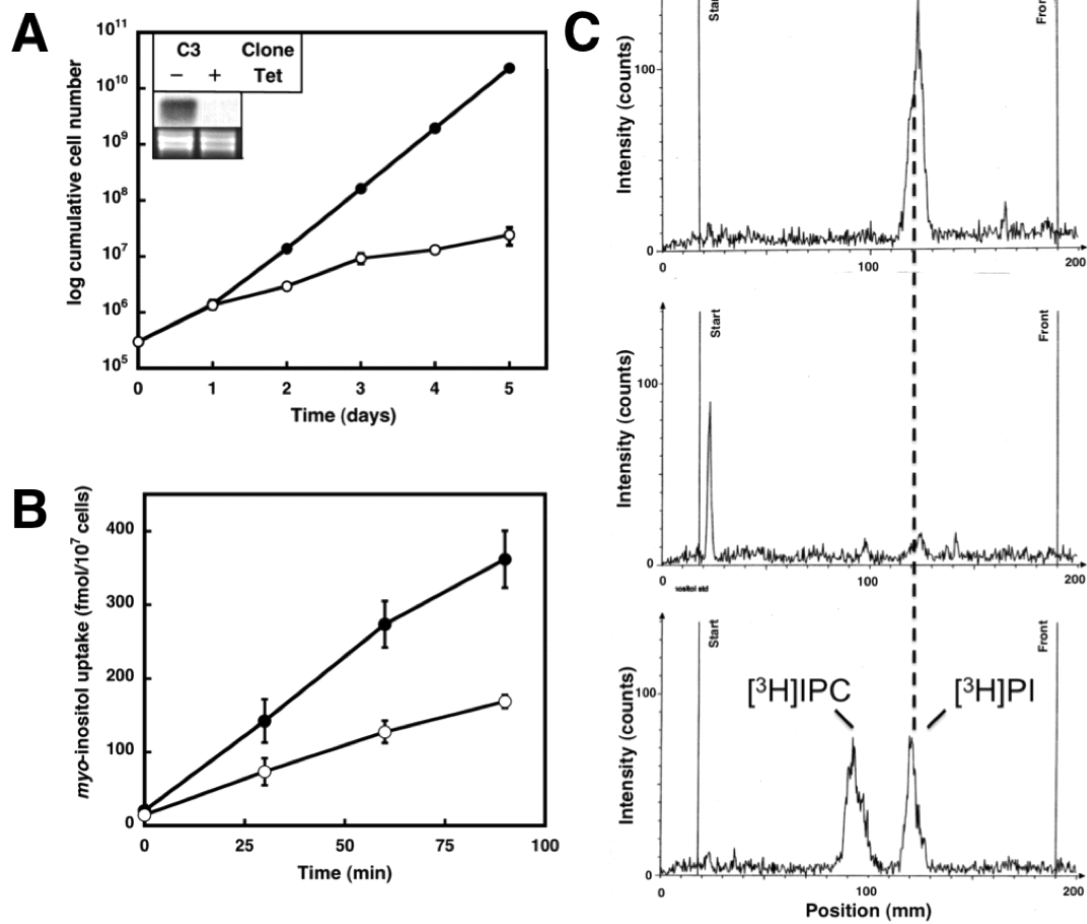
629 For details see main text. Glc-6-P, glucose-6-phosphate; GPI,
630 glycosylphosphatidylinositol; Ins, inositol; Ins-3-P, inositol-3-phosphate; IPC,
631 inositolphosphoryl ceramide; PI, phosphatidylinositol; TbHMIT, *T. brucei* H⁺-
632 coupled *myo*-inositol transporter; GlcNAc-PI, N-acetylglucosaminyl
633 phosphatidylinositol; GlcN-PI, glucosamine phosphatidylinositol; TbPIS, *T. brucei* PI
634 synthase; TbSLS1, *T. brucei* sphingolipid synthase 1; TbINO1, *T. brucei* 1-D-*myo*-
635 inositol-3-phosphate synthase; TbIMPase, *T. brucei* inositol monophosphatase.

636 **Figure 5. Structures of the various inositols and analogs tested in this study.** The
637 numbering refers to the parent *myo*-inositol numbering; the positions and substitutions
638 with a change relative to *myo*-inositol are indicated with the carbon number in blue
639 and highlighted in red color.

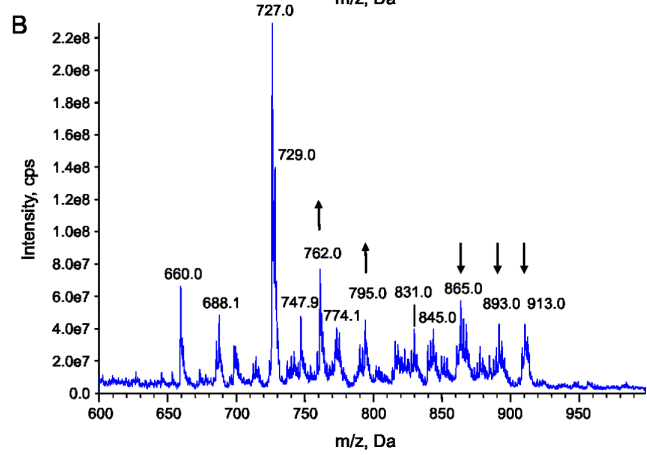
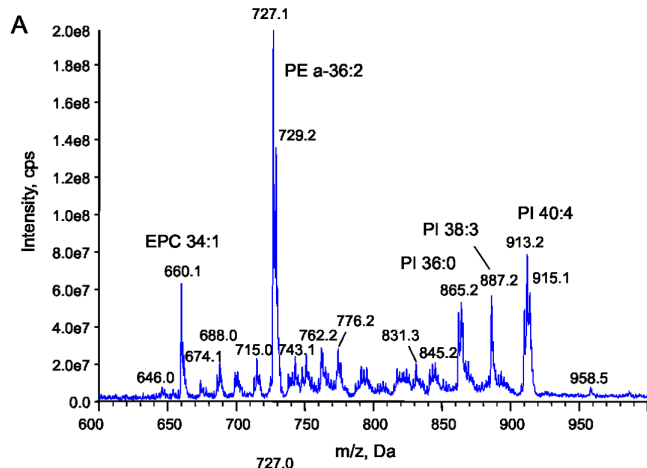
640 **Figure 6. Substrate specificity of TbHMIT.** *Xenopus* oocytes expressing TbHMIT
641 were exposed to 200 μ M *myo*-inositol and a series of structurally related compounds
642 (all at 200 μ M) and the currents were recorded. The bars indicate currents relative to
643 the response elicited by *myo*-inositol (mean values \pm standard deviations from at least

644 3 determinations). N-00601: (1R,4S)-6-methoxycyclohexane-1,2,3,4,5-pentol; N-
645 50350: (1R,3S)-6-methoxycyclohexane-1,2,3,4,5-pentol.

646

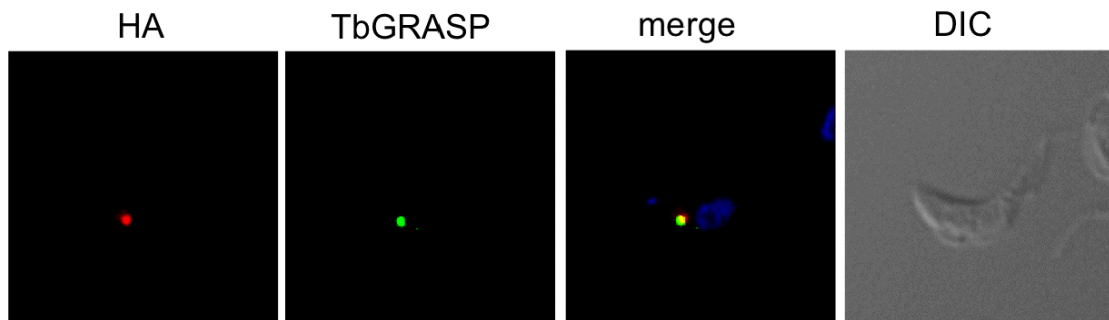


647



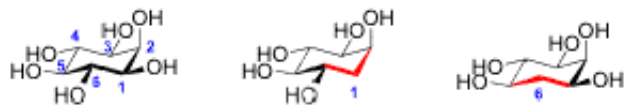
648

649



650

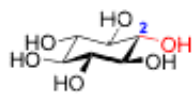
651



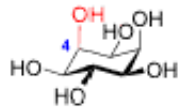
myo-inositol

(-)-*vibo*-quercitol

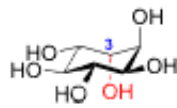
(+)-*epi*-quercitol



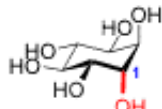
scyllo-inositol



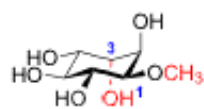
epi-inositol



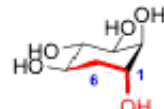
1L-*chiro*-inositol



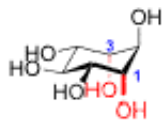
1D-*chiro*-inositol



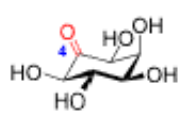
Quebrachitol



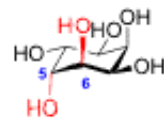
(+)-*proto*-quercitol



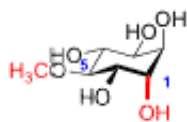
muco-inositol



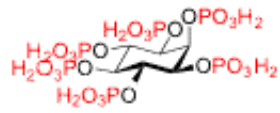
1L-*epi*-2-inosose



allo-inositol



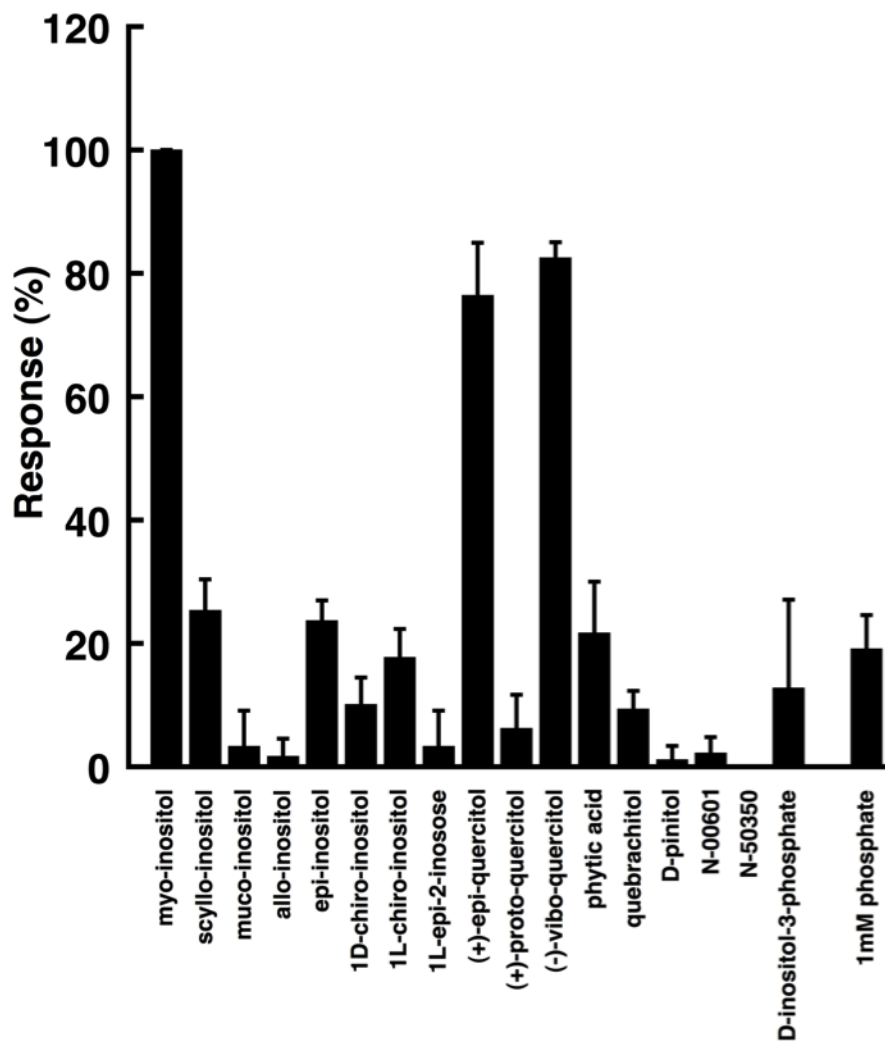
D-pinitol



phytic acid

652

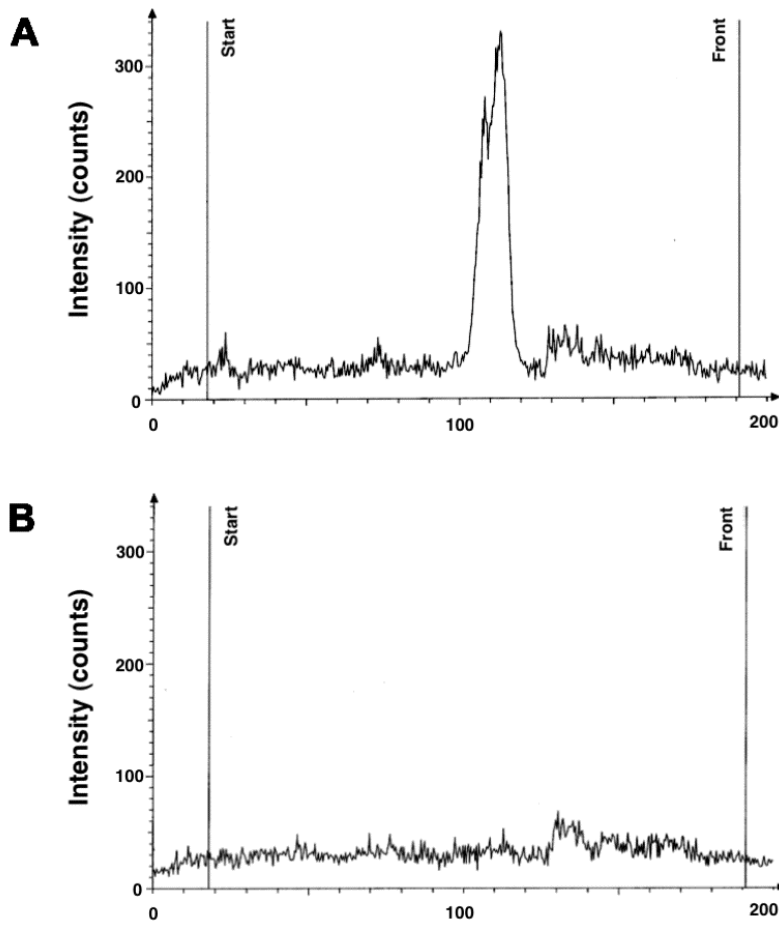
653



654

655 SUPPLEMENTARY FIGURES

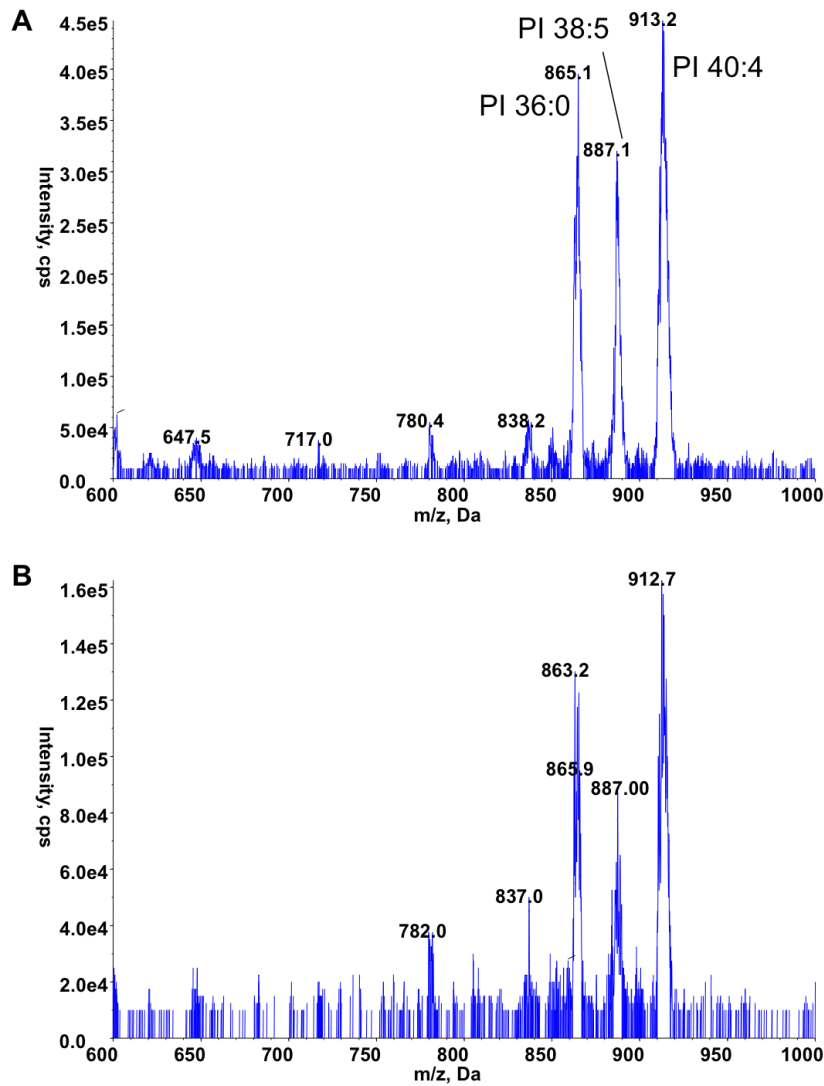
656



657

658

659 **Figure S1. Susceptibility of [³H]-labeled lipids to PI-PLC.** [³H]-labeled lipids were
 660 extracted from *T. brucei* bloodstream forms, incubated in the absence (upper panel) or
 661 presence (lower panel) of PI-PLC, and separated by one-dimensional TLC using
 662 solvent system 1. Radioactivity was detected by scanning the plate.



663

664

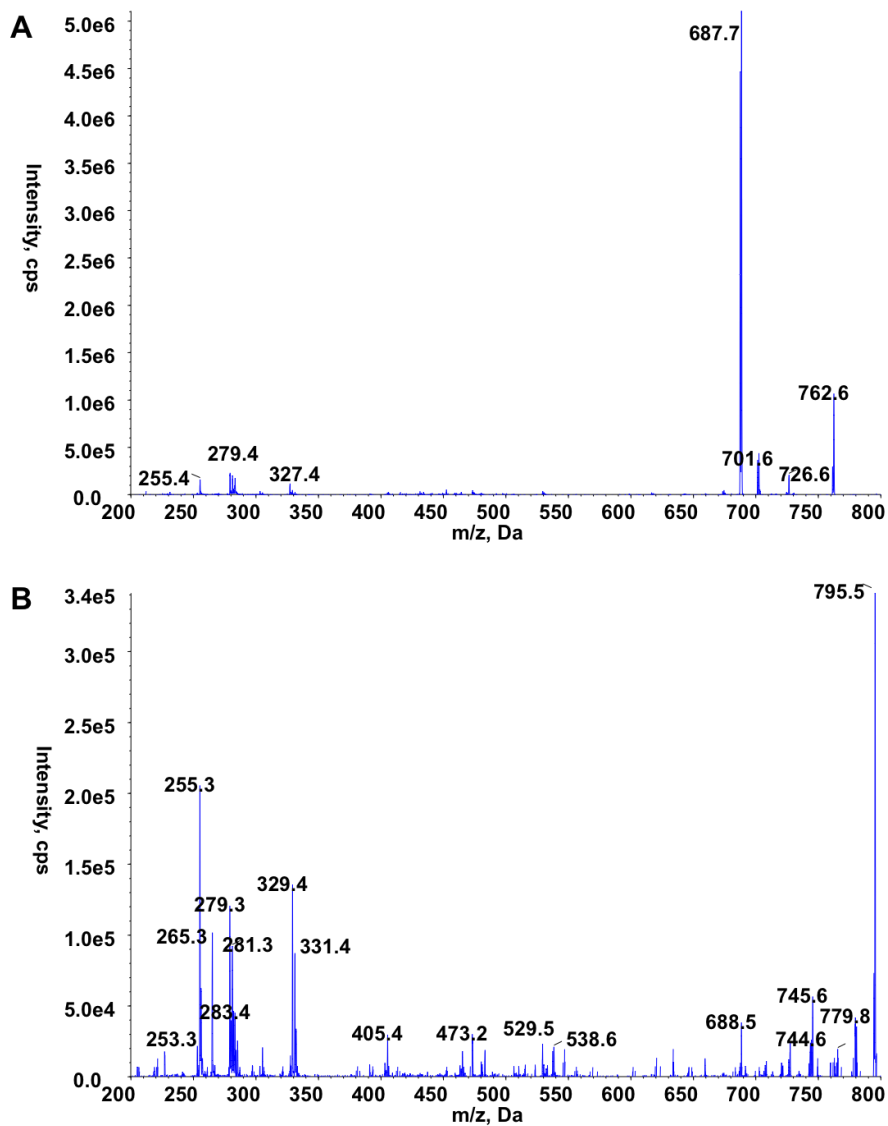
665 **Figure S2. Lipidomic analysis of inositol containing phospholipids from *T. brucei***

666 **TbHMIT RNAi knock-down cells by ES-MS-MS.** Lipid extracts from bloodstream

667 form parasites incubated in the absence (A) or presence (B) of tetracycline for 48

668 hours were analyzed by negative ion ES-MS-MS utilising parent ion scans of 241

669 (600-1000m/z).



670

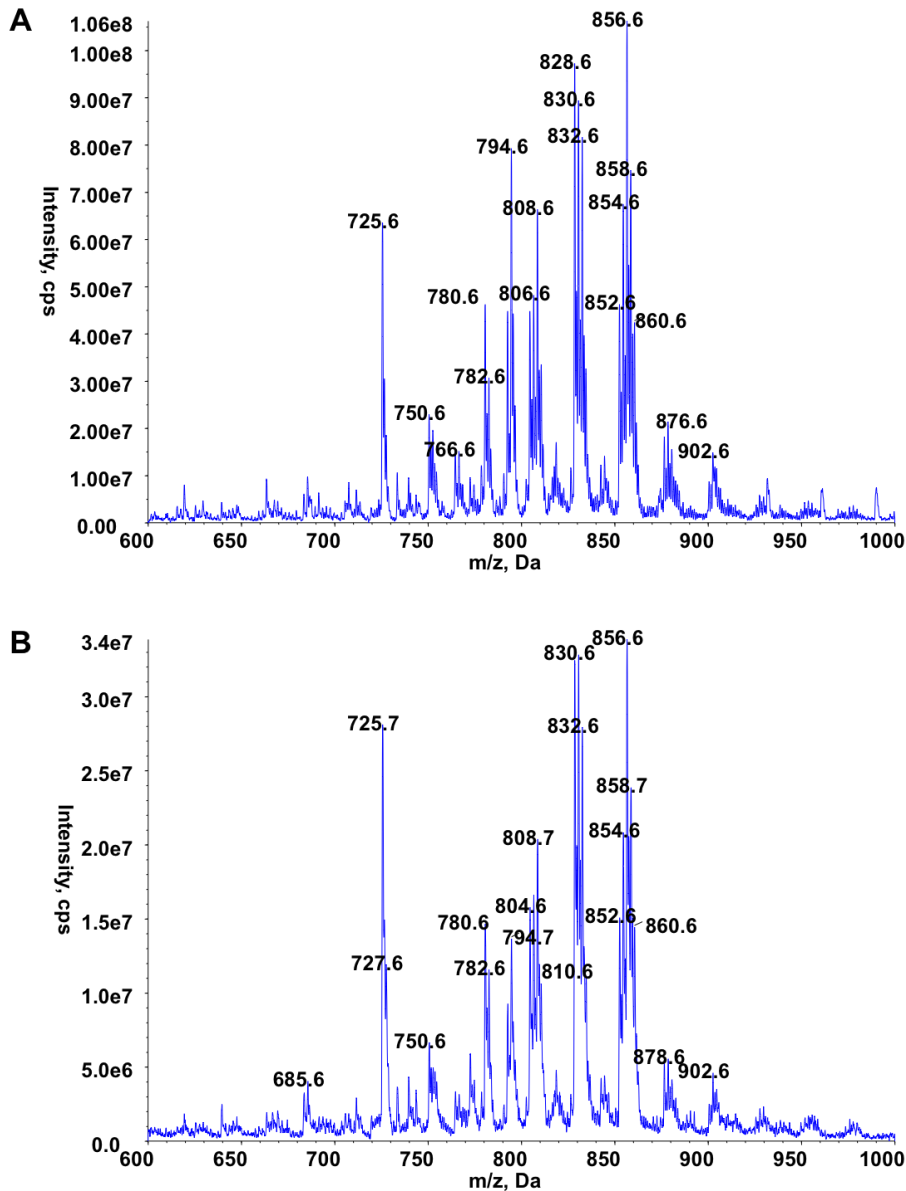
671

672 **Figure S3. Fragmentation of phospholipid species m/z 763 (A) and m/z 795 (B)**

673 **from *T. brucei* TbHMIT RNAi knock-down cells by ES-MS-MS. Fragmentation**

674 **reveals that (A) is mainly phosphatidylserine (34:0) and (B) is mainly**

675 **phosphatidylglycerol (38:5).**



676

677

678 **Figure S4. Positive ion ES-MS lipidomic analysis of *T. brucei* TbHMIT RNAi**

679 **knock-down cells.** Lipid extracts from bloodstream form parasites incubated in the

680 absence (A) or presence (B) of tetracycline for 48 hours were analyzed by positive ion

681 ES-MS survey scans (600-1000m/z).

682